Available online at www.sciencedirect.com

ScienceDirect

Geochimica et Cosmochimica Acta 145 (2014) 103–115

Geochimica et Cosmochimica Acta

www.elsevier.com/locate/gca

Variation of lithium isotope geochemistry during basalt weathering and secondary mineral transformations in Hawaii

Jong-Sik Ryu [a,*], Nathalie Vigier [b], Sin-Woo Lee [a], Kwang-Sik Lee [a], Oliver A. Chadwick [c]

[a] Division of Earth and Environmental Sciences, Korea Basic Science Institute, Chungbuk 363-883, South Korea
[b] LOV, CNRS, UPMC, UMR 7093, 181 chemin du Lazaret, 06230 Villefranche-sur-Mer, France
[c] Department of Geography, University of California, Santa Barbara, CA 93106, USA

Received 4 April 2014; accepted in revised form 24 August 2014; available online 30 September 2014

Abstract

Lithium isotopes are a potential tracer of silicate weathering but the relationship between lithium isotope compositions and weathering state still need to be established with precision. Here, we report Li concentrations and Li isotope compositions of soils developed along a 4 million year humid-environment chronosequence in the Hawaiian Islands. Li concentrations are variable with depth and age, ranging from 0.24 to 21.3 ppm, and significant Li depletions (up to 92%) relative to parent basalts are systematically enhanced towards the surface. Our calculations show that the relative contribution from atmospheric deposits to the Li soil budget remains small, with a maximum contribution from dust Li of 20% at the oldest site. This is explained by the capacity of the weathering products to retain, within the profiles, the Li coming from basalt alteration, and allows us to explore more specifically the role of alteration processes on soil Li isotope signatures. The δ^7Li values display a large range between −2.5‰ and +13.9‰. The youngest soils (0.3 ka) display the same δ^7Li value as fresh basalt, regardless of depth, despite ~30% Li loss by leaching, indicating that there is little Li isotope fractionation during the incipient stage of weathering. δ^7Li values for the older soils ($\geqslant$20 ka) vary non-linearly as a function of time and can be explained by progressive mineral transformations starting with the synthesis of metastable short-range order (nano-crystalline) minerals and followed by their transformation into relatively inert secondary minerals. Results highlight significant Li isotope fractionation during secondary mineral formation and in particular during Li uptake by kaolinite. Finally, we suggest that the non-monotonous evolution of the regolith δ^7Li value over the last 4 Ma is consistent with climatic variations, where congruent release of Li isotopes occurs during warmer periods.

1. INTRODUCTION

Chemical weathering of silicate rocks is an important regulator of the long-term global carbon cycle and therefore climate history (Walker et al., 1981; Dessert et al., 2001; Berner, 2004). In particular, basalt weathering accounts for about 35% of the global CO_2 sink associated with silicate weathering (Dessert et al., 2003), even though it covers a relatively small portion of Earth's surface. However, the key parameters and controlling factors of basalt weathering in nature are still debated (e.g., Gislason and Eugster, 1987; Gislason and Hans, 1987; Brady and Gíslason, 1997; Dessert et al., 2001, 2003).

* Corresponding author. Tel.: +82 43 2405334; fax: +82 43 2405319.
E-mail address: jongsikryu@gmail.com (J.-S. Ryu).

http://dx.doi.org/10.1016/j.gca.2014.08.030
0016-7037/

In this context, lithium isotopes of large rivers and oceans have potential as a proxy for tracing the type and intensity of silicate weathering (Huh et al., 1998, 2001; Vigier et al., 2009; Pogge von Strandmann et al., 2010; Misra and Froelich, 2012). Nevertheless, more work is required to provide clear linkages between fractionation processes occurring at the weathering profile scale with those inferred to be operating based on aqueous samples from large rivers. Experimental investigations have shown that basalt dissolution is not associated with significant isotope fractionation (Pistiner and Henderson, 2003; Wimpenny et al., 2010a; Verney-Carron et al., 2011) and that the formation of secondary phases, such as smectite and Fe oxides, leads to preferential enrichment of ^{6}Li into the weathering solids (Williams and Hervig, 2005; Vigier et al., 2008; Wimpenny et al., 2010b). The few existing studies of basaltic soils show that lithium isotopes hold great promise for tracing terrestrial weathering processes, but that the soil isotope signatures can be rapidly buffered by atmospheric deposits such as dust, rain or marine aerosols (Pistiner and Henderson, 2003; Huh et al., 2004; Kisakürek et al., 2004; Pogge von Strandmann et al., 2012; Liu et al., 2013). Here, we examine the processes responsible for changes in the Li isotope composition during progressive weathering and development of basaltic soils along a humid-environment chronosequence in the Hawaiian Islands. The exceptionally clear variations in lava flow ages and relatively stable variations in climate in Hawaii (Hotchkiss et al., 2000; Vitousek, 2004) provide a useful natural laboratory to evaluate non-traditional isotope systems as tracers of basalt weathering and/or vegetation recycling (e.g., Kennedy et al., 1998; Stewart et al., 2001; Pistiner and Henderson, 2003; Huh et al., 2004; Wiegand et al., 2005; Ziegler et al., 2005; Bern et al., 2010). This study focuses on the behavior of lithium isotopes during the initial stages of basalt weathering, and leaching through the slow accumulation of metastable secondary minerals and their reorganization into relatively inert secondary crystalline phases. We assess ways in which these various factors fractionate lithium isotopes into soil solids and the implications for isotopic signatures in streams fed by waters passing through the weathering profiles. Furthermore, we assess the role of atmospheric deposition and recent climate variations that could modify the soil isotopic signals.

2. STUDY AREA

The Hawaiian Islands are an ideal place to study the complex patterns of soil and ecosystem development imposed by variations in climate and lava-flow age (Porder and Chadwick, 2009; Porder et al., 2007; Vitousek and Chadwick, 2013). The Hawaiian chronosequence considered here varies in age from 0.3 to 4100 ka and has been referred to as the "Long-Substrate Age Gradient (LSAG)". Detailed descriptions of the LSAG are given in previous studies (e.g., Crews et al., 1995; Vitousek, 2004; Vitousek et al., 1997). All sites are near 1200 m elevation, receive 2500 mm annual rainfall, and have a mean annual temperature of 15 °C. The two youngest sites (0.3 ka; Thurston (Th) and Ola'a (Ol)) are in Keanakakoi tephra derived from phreatomagmatic eruptions of tholeiitic composition at the summit of Kilauea (McPhie et al., 1990; Fiske et al., 2009), while the older sites ($\geqslant$20 ka) are composed of alkali basalt, such as hawaiite, mugearite, and their associated tephra (MacDonald et al., 1983; Wright and Heltz, 1986; Wolfe and Morris, 1996). The soils exhibit a general trend of increasing crystallinity of secondary minerals with age (Chorover et al., 1999, 2004). In detail, the two youngest soils (0.3 ka) are Andisols composed primarily of glass, olivine, clinopyroxene, feldspar and magnetite–ilmenite. The three intermediate-aged soils (20, 150, and 1400 ka) are progressively more weathered Andisols with high concentrations of short-range-order materials, such as allophane, imogolite and ferrihydrite, whereas the oldest soil (4100 ka) is an Oxisol dominated by refractory secondary minerals, such as goethite, gibbsite, and kaolinite.

All soils are located on primary shield volcano surfaces, where physical erosion and groundwater influences are minimal. Erosion itself is nearly non-existent on Kilauea and Mauna Kea because the highly permeable lava flows have not yet been extensively capped by clay-rich soils that dramatically slow downward water flux and re-route it laterally (Lohse and Dietrich, 2005). On the older mountains, sampling sites are on constructional surfaces that are isolated on interfluves far from stream channels. None of the core sites has been cleared or systematically altered by direct human action. A fundamental assumption associated with this work is that the soil age approximates the age of the underlying lava flow. Although there is no definitive test of the assumption, research performed over the past two decades suggests it to be tractable. However it is reasonable to assume that there is a greater divergence between lava flow age and soil residence time as volcano age increases (for further discussions of this point see Vitousek et al., 1997; Hotchkiss et al., 2000; Kurtz et al., 2001; Vitousek, 2004).

3. MATERIALS AND METHODS

3.1. Sample preparation and chemical analysis

Soils were collected from hand-dug pits to about 1 m depth except for the youngest soil; Thurston (Th) is about 40 cm deep and overlies unweathered pahoehoe lava, and Ola'a (Ol) is about 70 cm deep and overlies a buried soil on the ~1000 year old Kulanaokuaiki tephra (Fiske et al., 2009; Fig. 1). All samples were air dried, passed through a 2-mm sieve, and then crushed in a shatter box equipped with a tungsten carbide grinding container. About 0.1 g of each sample was completely digested using concentrated, ultrapure HCl, $HClO_4$, HF, and HNO_3. The samples were dried, refluxed several times in 6.0 M HCl to remove fluorides, and re-dissolved in 5% HNO_3. Cation and trace element concentrations were measured using a Perkin Elmer Optima 4300DU ICP-AES and a Thermo Elemental X-7 ICP-MS, respectively at the Korea Basic Science Institute (KBSI). Accurate quantification was achieved by external calibration of the data relative to three USGS basalt standard powders (BCR-2, BHVO-2, and BIR-1).

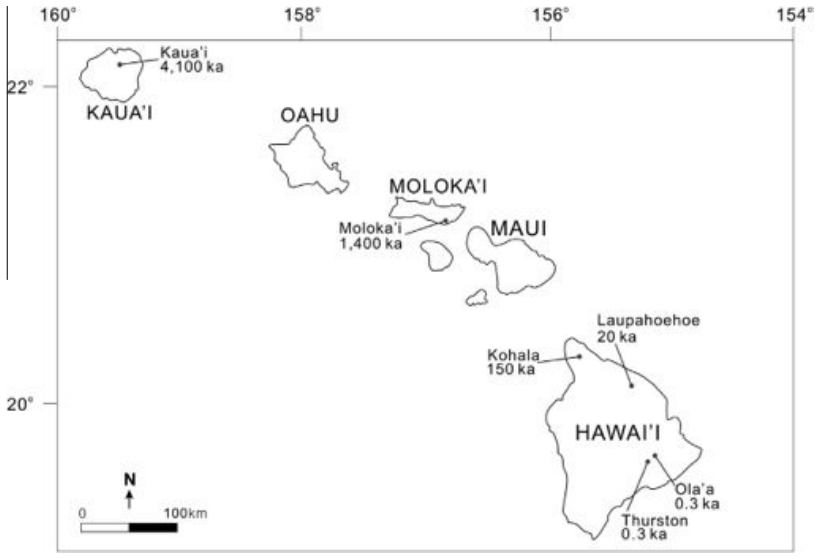

Fig. 1. Map of the Hawaiian Islands showing the sampling locations and their substrate ages (Modified from Crews et al., 1995).

3.2. Sr and Li isotope analyses

Strontium isotope ratios ($^{87}Sr/^{86}Sr$) were measured using a Neptune MC-ICP-MS at the KBSI. Samples were dried in Teflon vessels and re-dissolved in 8 M HNO_3. Strontium was separated from matrix elements using an Eichrom Sr resin following procedures described in Swoboda et al. (2008). The $^{87}Sr/^{86}Sr$ ratios were normalized to $^{86}Sr/^{88}Sr = 0.1194$, and the mean $^{87}Sr/^{86}Sr$ ratio of the NBS987 standard during analysis was 0.710247 ± 0.000008 (2σ, $n = 24$).

Detailed description of Li purification and its isotope measurement is given in Choi et al. (2013). In short, samples were dried in Teflon vessels, and the residues were treated with concentrated HNO_3, dried, and re-dissolved in a 1:4 (v/v) mixture of 6 M HNO_3 and 100% methanol. Li was separated from matrix elements using an AG 50W−X8 resin (200–400 mesh). After loading the sample, matrix elements were eluted with 4 mL of a 1:4 (v/v) mixture of 6 M HNO_3 and 100% methanol before collecting Li in 10 mL of a 1:4 (v/v) mixture of 6 M HNO_3 and 100% methanol. After Li purification, the sample was dried and re-dissolved in 5% HNO_3 (~40 ppb Li). Lithium isotope ratios were measured using a Neptune MC-ICP-MS under cool-plasma condition at the KBSI. Samples were introduced into a ~800 W plasma through a quartz dual cyclonic spray chamber, and analyzed using a blank-standard-blank-sample-blank-standard-blank bracketing method. Sample intensities were matched to within 10% of the intensity of the standard. The sensitivity was ~90 V/ppm on mass 7 at a typical uptake rate of 100 μL/min, and blank values were low (~30 mV for ^{7}Li; 0.8%). Prior to isotopic analysis, each sample was checked for yield and yields were greater than 95%. The Li isotopic composition is reported in delta notation relative to L-SVEC, where $\delta^7Li = [(^7Li/^6Li)_{sample}/(^7Li/^6Li)_{L\text{-}SVEC} - 1] \times 1000$. The accuracy and reproducibility of the whole method was validated using the USGS rock standards (BCR-2, BHVO-2, and BIR-1) and seawater standards (IAPSO and NASS-5). BCR-2 yielded $3.5 \pm 0.2‰$ (2σ, $n = 22$), BHVO-2 yielded $4.5 \pm 0.4‰$ (2σ, $n = 5$), BIR-1 yielded $3.3 \pm 0.6‰$ (2σ, $n = 5$), IAPSO yielded $30.9 \pm 0.2‰$ (2σ, $n = 29$), and NASS-5 yielded $30.6 \pm 0.5‰$ (2σ, $n = 15$), which were all in good agreement with reported values (e.g., You and Chan, 1996; Moriguti and Nakamura, 1998; Tomascak et al., 1999; Nishio and Nakai, 2002; Magna et al., 2004; Huang et al., 2010; Ludwing et al., 2011).

4. RESULTS

4.1. Li concentrations

Li concentrations ([Li]) in the soils are variable with depth and age, ranging from 0.24 to 21.3 ppm (Table 1). At the 0.3 ka sites (Th and Ol), [Li] in the surface horizons is 0.60 and 0.48 ppm, respectively, and increases to about 4 ppm for the deeper horizons, similar to tholeiitic basalt. At the 20 ka site, [Li] is low at the surface (0.43 ppm; 0–12 cm) and increases to about 4 ppm in the deeper horizons (average of 4.4 ppm; 20–110 cm), which is similar to values for tholeiitic basalt but much lower than that of alkali basalt (11 ppm; Huh et al., 2004). By contrast, at the 150 and 1400 ka sites, average [Li] are 14.9 and 9.8 ppm for all horizons (5–56 and 6–93 cm, respectively), except for the surface horizons, which are 2.0 and 1.1 ppm, respectively. The oldest 4100 ka site has average [Li] of 3.9 ppm for the top four horizons which reach to 60 cm depth, but from there to 105 cm the values increase to 7.7 and 9.7 ppm, relatively close to alkali basalt.

4.2. Li isotopes

The δ^7Li values span a wide range, from −2.5‰ for the 150 ka site to +13.9‰ for the 4100 ka site (Table 1). The youngest sites (0.3 ka) show little variation in δ^7Li

Table 1
Elemental and isotope geochemistry of bulk soil samples (<2 mm size fraction).

Sample	Age (ka)	Average depth (cm)	Density (ρ)[a] (g/cm^3)	K (%)	Mg (%)	Na (%)	Al (%)	Fe (%)	Sr (μg/g)	Li (μg/g)	Nb (μg/g)	δ^7Li[b] (‰)	^{87}Sr/^{86}Sr
T4 0–4	0.3	2	0.2	0.1	0.5	0.1	0.5	0.7	48.0	0.24	1.3	–	0.704525
T4 4–12		8	0.4	0.2	4.2	1.0	5.3	7.8	191	2.9	10	3.7	0.703779
T4 12–22		17	1.0	0.3	6.7	1.4	6.6	8.9	288	4.1	10	3.3	0.703805
T4 22–34		28	1.0	0.3	6.5	1.3	6.7	9.1	267	4.8	11	3.1	0.703694
T4 34–37		36	1.0	0.3	5.8	1.3	7.0	9.0	274	4.3	11	3.6	0.703720
T4 37–48		43	1.0	0.3	6.2	1.41	6.8	8.7	282	4.3	9	3.4	0.703700
T4 37–48-replicate				0.3	6.2	1.40	6.9	8.8	290	4.4	11	3.2	0.703699
OL5 0–5	0.3	3	0.2	0.2	1.1	0.2	1.5	1.7	63.5	0.60	2.4	3.9	0.704121
OL5 5–12		9	0.5	0.2	4.9	1.0	6.0	7.9	218	3.7	11	3.8	0.703868
OL5 20–28		24	1.0	0.3	8.8	1.5	9.4	12	322	5.1	12	3.4	0.703905
OL5 28–45		37	1.3	0.3	6.3	1.3	7.0	9.1	268	3.9	10	3.7	0.704114
OL5 45–62		54	1.3	0.3	6.4	1.37	7.1	9.2	299	4.4	11	3.6	0.704122
OL5 45–62-replicate				0.3	6.0	1.27	6.9	8.9	276	3.9	10	3.6	0.704138
LA1 0–12	20	6	0.3	0.1	0.1	0.0	0.8	2.0	8.59	0.43	7.7	–	0.706647
LA1 20–27		24	0.3	0.2	0.2	0.0	6.6	29	13.4	4.7	69	0.9	0.709703
LA1 52–94		73	0.5	0.1	0.6	0.0	13	13	4.61	4.7	52	−1.6	0.711514
LA1 94–110		102	0.6	0.0	1.7	0.00	15	11.3	4.32	4.1	59	2.6	0.706963
LA1 94–110-replicate				0.0	1.6	0.00	15	11.3	4.26	3.9	60	2.7	0.707165
KO2 0–5	150	3	0.3	0.2	0.2	0.1	1.1	1.6	25.9	2.0	33	4.7	0.710660
KO2 5–9		7	0.5	0.7	0.2	0.1	4.1	5.6	35.1	11.0	181	4.2	0.718436
KO2 15–26		21	0.6	1.7	0.4	0.2	6.7	8.5	67.5	21.3	365	5.3	0.720718
KO2 26–45		36	0.6	0.6	0.2	0.1	12	6.0	23.8	15.4	213	−0.1	0.719695
KO2 45–56		51	0.7	0.3	0.2	0.04	16	2.6	14.6	13.4	147	−2.4	0.717783
KO2 45–56-replicate				0.3	0.2	0.02	16	2.6	14.6	13.4	147	−2.6	0.717737
MK6 0–6	1400	3	0.3	0.1	0.2	0.1	1.2	1.3	45.2	1.1	38	7.6	0.708642
MK6 0–6-replicate												7.8	
MK6 6–18		12	0.4	0.5	0.4	0.1	14	16	143	12.9	350	4.7	0.706939
MK6 38–55		47	0.7	0.1	0.2	0.0	19	6.5	58.2	9.5	85	2.5	0.704983
MK6 55–74		65	0.8	0.0	0.1	0.0	23	4.4	50.7	8.6	47	0.6	0.704507
MK6 74–93		84	1.0	0.0	0.1	0.01	22	5.1	49.2	8.4	48	1.8	0.704516
MK6 74–93-replicate				0.0	0.1	0.03	23	5.3	51.3	9.4	50	1.9	0.704471
KAI3 0–5	4100	3	0.3	0.1	0.3	0.0	4.0	19	114	3.8	273	13.8	0.706818
KAI3 0–5-replicate												14.0	
KAI3 16–22		19	0.9	0.1	0.1	0.0	9.1	40	152	4.6	262	6.0	0.706001
KAI3 22–34		28	0.8	0.1	0.1	0.0	8.7	30	129	3.2	194	6.5	0.705932
KAI3 34–60		47	1.1	0.0	0.1	0.0	16	18	240	4.2	116	3.2	0.705085
KAI3 60–86		73	1.2	0.0	0.3	0.0	14	12	82.7	7.7	105	2.4	0.705338
KAI3 86–105		96	1.2	0.0	0.7	0.00	16	13.4	202	10.8	105	3.8	0.704546
KAI3 86–105-replicate				0.0	0.7	0.00	16	13.60	207	8.5	108	3.9	0.704593

The external precisions of δ^7Li and ^{87}Sr/^{86}Sr are better than 0.6‰ (2σ) and 8 ppm (2σ), respectively (see text for more details).
[a] Data from Pett-Ridge et al. (2007).
[b] Not determined.

(3.5 ± 0.5‰, 2σ, $n = 10$), in good agreement with previous results (Pistiner and Henderson, 2003). These δ^7Li values are consistent with values for Hawaiian basalt (4.0 ± 0.9‰; Tomascak et al., 1999; Chan and Frey, 2003; Pistiner and Henderson, 2003), and more generally with fresh MORB and OIB values (3.7 ± 2.1‰; Tomascak et al., 2008; Krienitz et al., 2012). At the 20 ka site, δ^7Li ranges between −1.6‰ for the deeper horizons (52–94 cm) and 2.6‰ for the deepest one. At the 150 ka site, δ^7Li ranges from 4.2‰ to 5.3‰ in the near-surface horizons (0–26 cm) but decreases to −2.5‰ at about 50 cm depth. At the two oldest sites, δ^7Li is highest at the surface (7.7‰ and

13.9‰, respectively) and then decreases to 1.8‰ and 3.8‰, respectively, with depth.

5. DISCUSSION

5.1. Li mobility during basalt alteration

Intense weathering of basalt can result in redistribution of even the most refractory elements, such as Hf, Th and Zr (Kurtz et al., 2000). As elements are being leached the remaining element configurations become more stable: soil minerals evolve first to nano-crystalline gibbsite, allophane and ferrihydrite (SRO minerals) and then to crystalline products, such as goethite, gibbsite and kaolinite (Vitousek et al., 1997; Chorover et al., 2004; Ziegler et al., 2005). The relative gain ($\tau_{j,w} > 0$) or loss ($\tau_{j,w} < 0$) of each major and minor element along the chronosequence can be estimated as follows (Brimhall and Dietrich, 1987; Chadwick et al., 1990):

$$\tau_{j,w} = \frac{C_{j,w} \times C_{i,p}}{C_{j,p} \times C_{i,w}} - 1, \quad (1)$$

where C is the concentration of an element, w and p refer to the weathered and parent materials, respectively, and i and j refer to the immobile and mobile elements, respectively. In this study, we use Nb as the index element because Nb most closely approximates element immobility in Hawaiian weathering profiles (Kurtz et al., 2000).

Fig. 2a shows that in the surface horizons, τ_{Li} decreases from 0.3 to 4100 ka (from −51% to −92%), indicating progressive loss of Li with age. Even in the two youngest soils, the surface is depleted in Li compared to parent basalt. Part of this depletion could be due to dilution by Li-poor phases, such as organic matter (OM). However, Li is normalized to Nb (Eq. (1)), which should minimize this effect, and also we note that the OM content of the surface horizons does not increase linearly with age (Ziegler et al., 2005). Instead, we think that because the complexation of Al by organic matter (in OM-Al) often occurs in the surface horizons of volcanic soils, the associated lack of clay mineral formation in the surface could minimize Li retention in these horizons. As a consequence, Li released by weathering in the surface and/or from decomposition of OM moves deeper into the profile before it can be captured during clay mineral synthesis. Below 40 cm depth, τ_{Li} increases with depth, indicating a significant enrichment relative to the surface horizons. This feature is likely related to limited basalt weathering for the two youngest soils (0.3 ka) and to clay mineral formation at depth for the older soils ($\geqslant$20 ka). A significant increase in the relative abundance of kaolin (primarily halloysite) can account for the Li enrichment observed at the two oldest sites (Table S1; Vitousek et al., 1997; Ziegler et al., 2005) because kaolin minerals can contain significant amounts of Li (Tardy et al., 1972).

Depth-integrated τ_{Li} allows us to calculate the total loss or gain of Li and other elements over the timescale of each profile as follows:

$$\tau_{int} = \frac{\sum(\tau_h \cdot \rho_h \cdot z_h)}{\sum(\rho_h \cdot z_h)}, \quad (2)$$

where τ_h is the $\tau_{j,w}$ value of each horizon (h; Eq. (1)), z_h is horizon thickness, and ρ_h is horizon density taken from Pett-Ridge et al. (2007). As illustrated in Fig. 3, τ_{int} for alkali elements (Na and K) are negative at all sites and the older sites ($\geqslant$20 ka) have average τ_{int} close to −100%, indicating that both Na and K are completely depleted after 20 ka (Vitousek et al., 1997). In contrast, τ_{int} for Li, which is similar to τ_{int} for Na and K before 20 ka, remains significantly elevated (between −58% and +3%) between 20 and 4100 ka relative to Na and K. This strongly suggests that Li is less mobile than other alkali elements. Also, it is interesting to note that Li is less mobile than Mg after 20 ka even though they have similar ionic radius (Huh et al., 1998). The high τ_{int} for Li relative to Na or K at the older sites ($\geqslant$20 ka) suggests a key role of Li-rich but alkali- and Mg-poor secondary phases (Chorover et al., 2004). The Li enrichment at the two oldest sites (1400 and 4100 ka) can be explained by progressive accumulation of kaolin, but other phases may also play a role: (1) poorly- and non-crystalline phases that are abundant at the 20, 150 and 1400 ka sites, and (2) sesquioxides that are particularly abundant at the 20 and 4100 ka sites (Table S1; Chorover et al., 2004; Ziegler et al., 2005). Furthermore, the 1400 ka soil contains much more kaolin than the 150 ka soils, and more non-crystalline phases than the 4100 ka soil (Table S1), indicating that the particularly high τ_{Li} at the 1400 ka site is due to these mineralogical differences. Another possibility is that the Li excess can be partly explained by a significant contribution from atmospheric deposition, such as dust and rainwater.

5.2. Quantifying the relative role of alteration and atmospheric deposition in the Li budget

Previous work has shown that with age basalt weathering becomes relatively less important to the soil budget of some specific elements like Sr and atmospheric inputs become more important (Kurtz et al., 2001; Chadwick et al., 2009). For the Hawaiian Islands Long Substrate Age Gradient (LSAG; Crews et al., 1995), the roles of biogeochemical cycling and of Asian dust accretion in determining the fate of specific elements have been evaluated using Ca, Nd, Si, and Sr isotopes (Kennedy et al., 1998; Kurtz et al., 2001; Wiegand et al., 2005; Ziegler et al., 2005; Chadwick et al., 2009). In particular, Sr and Nd isotopes allow quantitative estimation of Asian dust and rainwater contribution. For example, Chadwick et al. (2009) indicated that basalt weathering clearly controls Sr isotopic composition at the two youngest sites (0.3 ka), and that atmospheric deposits become significant for Sr at the 20 ka site and are particularly abundant at the 150 ka site. Rainwater also provides a significant part of the labile Sr utilized by ecosystems, while dust minerals, in particular quartz, weather slowly, leading to a small influence. At the oldest site, a refractory secondary mineral with a Fe, Ti spinel-structure containing alkaline earth elements could protect basaltic Sr. It appears that basalt-derived Sr contributes more than expected due to this “chemical” protection whereas dust contributes less because it has been eroded from the surface (Chadwick et al., 2009). Kurtz

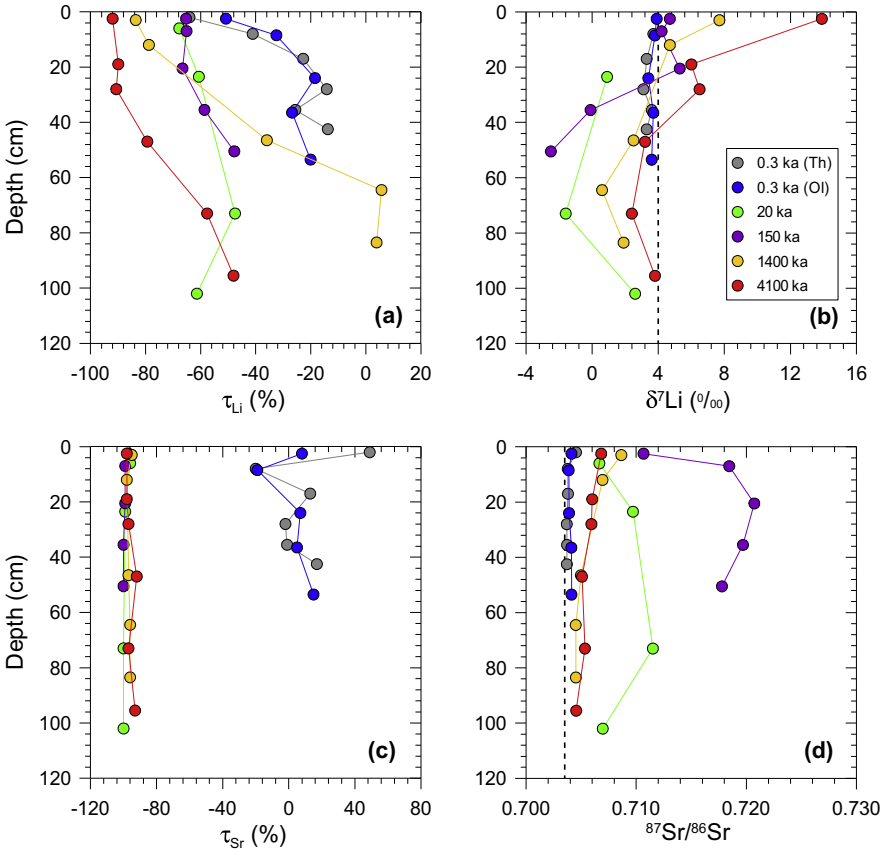

Fig. 2. The elemental gain ($\tau_{j,w} > 0$) or loss ($\tau_{j,w} < 0$), and isotope compositions versus depth. (a and c) τ_{Li} and τ_{Sr} are calculated using Eq. (1). The 0.3 ka sites are developed on a tholeiitic lava flow ([Li] = 5.6 ppm; Chan and Frey, 2003, [Nb] = 11 ppm; Pett-Ridge et al., 2007, [Sr] = 270 ppm; Chadwick et al., 2003), while the other sites are developed on hawaiites ([Li] = 11 ppm; Huh et al., 2004, [Nb] = 63 ppm; Pett-Ridge et al., 2007, and [Sr] = 1615 ppm; Chadwick et al., 2003) (see text for more details). (b and d) The external precisions of δ^7Li and ^{87}Sr/^{86}Sr are better than 0.6‰ (2σ) and 8 ppm (2σ), respectively (see text for more details). The dotted lines represent average δ^7Li of 4.0‰ (b) and ^{87}Sr/^{86}Sr of 0.7035 (d) of Hawaiian basalts.

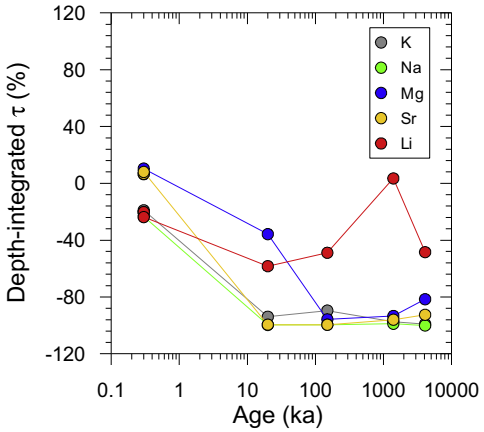

Fig. 3. Depth-integrated τ values in the total regolith for K, Na, Mg, Sr, and Li versus age. Depth-integrated τ is calculated using Eq. (2) (see text for more details).

et al. (2001) also reported similar results to Chadwick et al. (2009) but with a difference at the 150 ka site, where a mixture of basalt weathering and dust input controls Nd isotopes.

Fig. 2d shows that, except for the two youngest sites, the ^{87}Sr/^{86}Sr ratios are significantly higher than that of parent basalt, indicating a significant contribution from rainwater and/or dust. This effect is particularly clear at the 150 ka site, which exhibits the most radiogenic ^{87}Sr/^{86}Sr ratio of ~0.72 for the near-surface horizons (~20 cm). However, there is no correlation between δ^7Li and ^{87}Sr/^{86}Sr (not shown). These horizons do not exhibit δ^7Li signatures that are closer to rainwater (δ^7Li = 14.3‰; Pistiner and Henderson, 2003) or to dust (δ^7Li = 1.7‰; upper continental crust (UCC); Teng et al., 2009). Also, if the dust input was significantly enhanced with age, there should be negative correlation between content of quartz + mica and δ^7Li because quartz and mica are uniquely associated with continental dust in Hawaii (Rex et al., 1969; Jackson et al., 1971; Porder et al., 2007). However, from reported mineralogical composition (Table S1; Ziegler et al., 2005), there is no correlation between them, suggesting that the dust input is not a primary control of Li isotopic compositions in the Hawaiian soils.

Table 2
Summary of results for Li mass-balance calculation.

Age (ka)	Regolith thickness[a] (m)	Collapse factor (S_c)[b]	τ_{int_Li}[c] (%)	$Li_{present}$[d] (mg/cm^2)	Li_{total}[e]			Li_{loss}[f] (mg/cm^2)
					Li_{basalt} (mg/cm^2)	Li_{dust} (mg/cm^2)	$Li_{rainwater}$ (mg/cm^2)	
0.3 (Th)	0.4	0.6	−20	0.17	0.21	0.000	0.000	0.04 ± 0.00
0.3 (Ol)	0.6	0.8	−24	0.23	0.35	0.000	0.000	0.12 ± 0.00
20	2	0.4	−58	0.37	1.1	0.067 ± 0.021	0.003 ± 0.007	0.76 ± 0.03
150	4	1.3	−49	3.7	7.4	0.50 ± 0.15	0.02 ± 0.05	4.3 ± 0.2
1400	22	0.6	3	19	19	4.7 ± 1.4	0.19 ± 0.46	4.7 ± 1.9
4100	40	1.6	−48	46	89	14 ± 4	0.56 ± 1.4	58 ± 6

Two standard deviation (2σ) is propagated using the range of Li concentration for each end-member.
Li concentration in dust is assumed to be either UCC ([Li] = 24 ppm; Rudnick and Gao, 2003) or loess ([Li] = 29.8 ppm; Teng et al., 2004). Li concentration in Hawaiian rainwater is assumed to be either [Li] = 75×10^{-6} (filtered) or 1014×10^{-6} (unfiltered) ppm (Pistiner and Henderson, 2003).

[a] Informed estimates (see text for more details).
[b] Collapse factor is the ratio of the present Nb inventory in the regolith ($Nb_{regolith}$) to the total Nb coming from the parent basalt (Nb_{basalt}).
[c] Depth-integrated τ value in the regolith (see text for more details).
[d] $Li_{present}$ is the depth-integrated Li based on measured Li concentration, regolith thickness and density (see text for more details).
[e] The 0.3 ka regoliths are developed in tholeiitic tephra ([Li] = 5.6 ppm; Chan and Frey, 2003, and [Nb] = 11 ppm; Pett-Ridge et al., 2007), while the others are developed on hawaiites ([Li] = 11 ppm; Huh et al., 2004, and [Nb] = 63 ppm; Pett-Ridge et al., 2007).
[f] $Li_{loss} = Li_{total} - Li_{present}$ (see text for more details).

The Li contribution from Asian dust can be estimated more precisely for each profile because the elemental composition of the dust in Hawaii has remained relatively invariant during the past 4100 ka (Kyte et al., 1993) as follows:

$$Li_{dust} = C^{Li}_{dust} \cdot F_{dust} \cdot t, \quad (3)$$

where C^{Li}_{dust} is the average Li concentration in upper continental crust (24 ppm; Rudnick and Gao, 2003), F_{dust} is the average long-term dust deposition rate for Hawaii (30 mg/cm^2/ka for the younger soils (<20 ka) and 125 mg/cm^2/ka for the older soils (⩾20 ka); Kurtz et al., 2001), and t is the age of the soil site. The mass of dust-derived Li ranges between 0.22 μg/cm^2 at the 0.3 ka sites and 12 mg/cm^2 at the 4100 ka site (Table 2). Assuming that the Li concentration of dust is close to that of loess (29.8 ppm; Teng et al., 2004), it would lead to slightly higher values, ranging from 0.27 μg/cm^2 at the 0.3 ka sites to 15 mg/cm^2 at the 4100 ka site.

Similarly, the atmospheric Li input linked to rainwater can be calculated as follows:

$$Li_{rainwater} = C^{Li}_{rainwater} \cdot MAP \cdot t, \quad (4)$$

where $C^{Li}_{rainwater}$ is the Li concentration in filtered Hawaiian rain (0.075 ng/cm^3; Pistiner and Henderson, 2003) and MAP is the Mean Annual Precipitation (2500 mm/yr). The calculated mass of rainwater-derived Li ranges from 5.6 ng/cm^2 at the 0.3 ka sites to 77 μg/cm^2 at the 4100 ka site (Table 2). Instead, the unfiltered rainwater Li concentration (1.01 ng/cm^3; Pistiner and Henderson, 2003) provides a maximum estimate, which ranges from 76 ng/cm^2 at the 0.3 ka sites to 1.0 mg/cm^2 at the 4100 ka site. The rainwater Li input is systematically lower than the dust Li input with the ratio of rainwater Li to dust Li ranging from 2.1% for the two youngest sites to 0.5% for the other sites (⩾20 ka).

Since the sites exhibit minimal physical erosion, the overall weathering thickness should be directly linked to their age (e.g., Pett-Ridge et al., 2007). In this context, the quantity of Li released from the parent basalt can be estimated as follows:

$$Li_{basalt} = C^{Li}_{basalt} \cdot z_t \cdot S_c \cdot \rho_{basalt}, \quad (5)$$

where C^{Li}_{basalt} is the Li concentration in basalt (5.6 ppm in tholeiitic basalt for the two youngest sites and 11 ppm in alkali basalt for the older sites; Chan and Frey, 2003; Huh et al., 2004), z_t is the total regolith thickness (m), ρ_{basalt} is the average density of basalt including void and infilled vesiculated tephra (1.25 g/cm^3; Huh et al., 2004), and S_c is the collapse factor (Table 2). Total regolith thickness is difficult to determine even in cases where a backhoe or drill is available because of local variability related to void spaces and hydrological permeability (Goodfellow et al., 2013). We do however have several observations that allow us to make rough estimates as follows: 0.3 ka = 0.4 (Th) and 0.6 (Ol) m, 20 ka = 2 m, 150 ka = 4 m, 1400 ka = 22 m, and 4100 ka = 40 m (Table 2). Results show that the mass of Li released from the parent basalt ranges between 0.21 mg/cm^2 at the 0.3 ka site (Th) and 89 mg/cm^2 at the 4100 ka site (Table 2; Fig. 6a). Eqs. (3)–(5) allow us to calculate the total Li in the regolith, which is the sum of Li released from the parent basalt, with Li added from dust and rainwater along the course of the regolith development as follows:

$$Li_{total} = Li_{basalt} + Li_{dust} + Li_{rainwater}, \quad (6)$$

Li_{total} in the regolith increases continuously with age, ranging from 0.21 mg/cm^2 for the 0.3 ka site (Th) to 102 mg/cm^2 at the 4100 ka site (Table 2; Fig. 6a). The

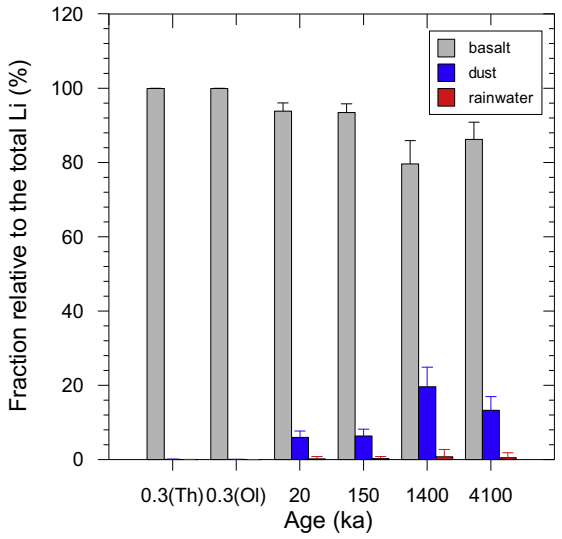

Fig. 4. Fraction of each end-member (basalt, dust, and rainwater) relative to the total Li (%) versus age. Error bars represent 2σ, propagated using the range of Li concentrations for each end-member (see text for more details).

relative contribution of each source is shown in Fig. 4, where the parent basalt provided between 80% and 100% of Li_{total}, rainwater a maximum of 0.8% (at 1400 ka), and dust becomes significant from 20 and 150 ka (~6%) and reaches at maximum 20% of Li_{total} at 1400 ka.

It is possible to compare Li_{total} corresponding to the regolith residence time, to the Li currently present in the regolith, $Li_{present}$ (i.e., depth-integrated Li mass per unit area). The difference between these two parameters allows the Li released, Li_{loss}, by the profile to the waters to be evaluated as follows:

$$Li_{present} = \sum_h \left(\rho_h \cdot z_h \cdot C_h^{Li}\right) \quad (7)$$

$$Li_{loss}(\%) = \left[Li_{present}/(Li_{basalt} + Li_{dust} + Li_{rainwater}) - 1\right] \times 100 \quad (8)$$

where C_h^{Li} is the Li concentration in the each soil horizon. At each site, $Li_{present}$ represents the depth-integrated Li, and is systematically lower than Li_{total} (Table 2; Fig. 6a), highlighting a significant Li loss at all the sites. This loss is likely due to weathering, dissolution, and leaching by soil waters. These results are in good agreement with depth-integrated τ values (Fig. 3). We thus confirm that all the sites have lost some Li, between 19% at the 0.3 (Th) and 1400 ka sites, and 67% at the 20 ka site.

5.3. Impact of atmospheric deposition on Li isotopes

The same approach can be applied to quantify the impact of dust and rainwater on δ^7Li values. Indeed, dust and rainwater have different Li isotope compositions relative to basalt, and therefore, even small amounts of these two end-members may affect the soil Li isotope composition. Based on our previous estimates of Li_{dust} and Li_{rain} (Table 2), we can quantify how the δ^7Li value of the total Li, δ^7Li_{total}, has varied with age as follows:

$$\delta^7Li_{total} = \left(\frac{\delta^7Li_{basalt} \cdot Li_{basalt} + \delta^7Li_{dust} \cdot Li_{dust} + \delta^7Li_{rainwater} \cdot Li_{rainwater}}{Li_{basalt} + Li_{dust} + Li_{rainwater}}\right), \quad (9)$$

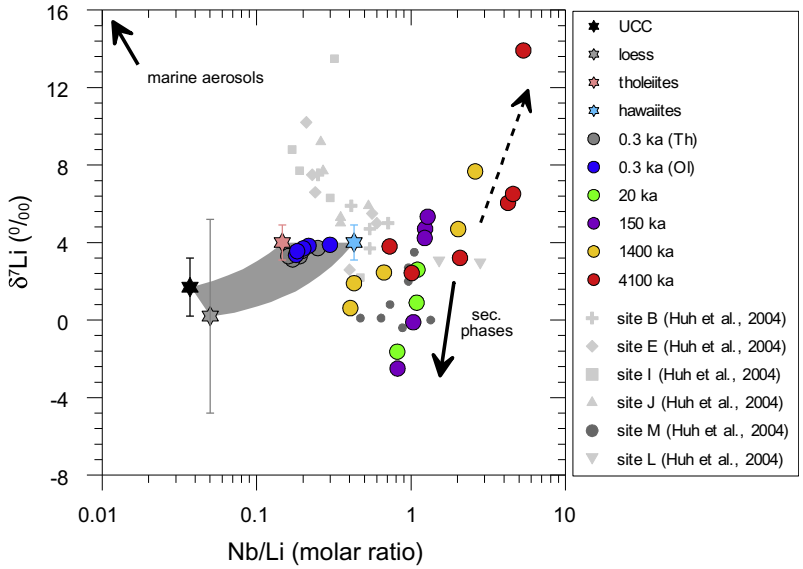

Fig. 5. δ^7Li values versus the molar Nb/Li ratio for all soil samples measured in this study. The upper continental crust has a δ^7Li of $1.7 \pm 1.5‰$ with a molar Nb/Li ratio of 0.04 (Teng et al., 2004, 2009), loess δ^7Li is $0.2 \pm 5.0‰$ with a molar Nb/Li ratio of 0.05 (Teng et al., 2004, 2009), rainwater δ^7Li is $31 \pm 0.5‰$ (Millot et al., 2007) with a molar Nb/Li ratio of 1.2×10^{-4}, and tholeiites and hawaiites δ^7Li are $4.0 \pm 0.9‰$ (Tomascak et al., 1999; Chan and Frey, 2003; Pistiner and Henderson, 2003) with a molar Nb/Li ratio of 0.15 and 0.43, respectively. The gray shaded field marks the mixing zone between each considered end-member, except for marine aerosols highlighted by the black arrow. Data for sites B–L are from Huh et al. (2004).

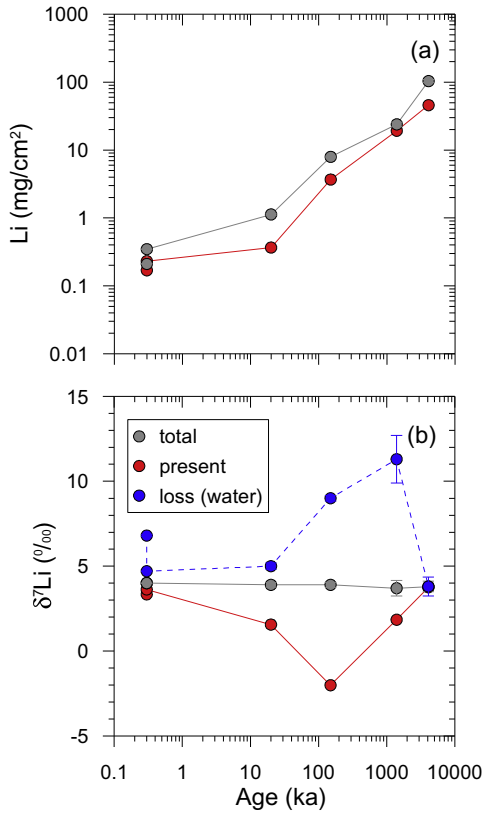

Fig. 6. Li mass per unit area basis (a) and δ^7Li values (b) versus age. The total Li (in gray) is the sum of Li coming from the parent basalt, and Li added from dust and rainwater. The present Li (in red) represents the depth-integrated Li based on measured Li concentration, total regolith thickness and density (Table 2). δ^7Li of the present Li is the depth-integrated δ^7Li value measured for each profile. See text for corresponding mass balance calculations. Error bars represent 2σ, and some of the error bars are smaller than the symbols. (For interpretation of the references to color in this figure legend, the reader is referred to the web version of this article.)

where $\delta^7Li_{basalt} = 4.0‰$ (Hawaiian basalts; Tomascak et al., 1999; Chan and Frey, 2003; Pistiner and Henderson, 2003), $\delta^7Li_{dust} = 1.7‰$ (UCC; Teng et al., 2009), and $\delta^7Li_{rainwater} = 31‰$ (seawater; Millot et al., 2007). Table 3 summarizes results and Fig. 6b shows that, despite significant contribution from dust to the older sites, the δ^7Li value of Li_{total} has remained constant, close to δ^7Li of the basalt (~4‰) over 4100 ka. This suggests a negligible influence of atmospheric deposits (both dust and rainwater) on the Li isotope composition of regolith. The result is significantly different from previous results showing that there is a significant influence of atmospheric deposits in Hawaii (Pistiner and Henderson, 2003; Huh et al., 2004), or in other basaltic environments (Kisakürek et al., 2004; Pogge von Strandmann et al., 2012; Liu et al., 2013). The correlation between δ^7Li value and molar Nb/Li exhibited by the Hawaiian soils studied here supports these calculations (Fig. 5). Indeed, except for the two youngest sites that have

Table 3
Summary of results for δ^7Li mass-balance calculations.

Age (ka)	$\delta^7Li_{present}$ [a] (‰)	δ^7Li_{total} [b] (‰)	δ^7Li_{loss} [b] (‰)
0.3 (Th)	3.3	4.0 ± 0.0	6.8 ± 0.0
0.3 (Ol)	3.6	4.0 ± 0.0	4.7 ± 0.0
20	1.6	3.9 ± 0.1	5.0 ± 0.2
150	−2.0	3.9 ± 0.1	9.0 ± 0.2
1400	1.8	3.7 ± 0.5	11.3 ± 1.4
4100	3.8	3.8 ± 0.3	3.8 ± 0.6

Two standard deviation (2σ) is propagated using uncertainties on the Li flux for each end-member.
$\delta^7Li_{basalt} = 4.0‰$ (Hawaiian basalt; Tomascak et al., 1999; Chan and Frey, 2003; Pistiner and Henderson, 2003).
$\delta^7Li_{dust} = 1.7‰$ (upper continental crust; Teng et al., 2009).
$\delta^7Li_{rainwater} = 31‰$ (seawater; Millot et al., 2007).
[a] Depth-integrated δ^7Li value in the regolith (see text for more details).
[b] Calculated using the results in Table 2 and standard isotope mass-balance equation (see text for more details).

Li isotope composition similar to the parent rocks, none of the soil samples can be explained by a simple mixing between a basalt and dust or rainwater end-members. By comparison, the Hawaiian soils sampled along a climosequence studied by Huh et al. (2004) exhibit a distinctly different trend, compatible with a significant contribution from marine aerosols (Fig. 5). However, their site M, developed at the same elevation and under the same precipitation rate as the chronosequence ones, displays essentially a weathering trend, mainly controlled by basalt alteration (Fig. 5). The contrast between the Kohala climosequence and the LSAG chronosequence suggests that our estimations of the Li mass balance for our sites are reasonable. In addition, simple calculations also show that the high δ^7Li value measured in some of the soil horizons cannot be explained by the mixing of atmospherically derived Li with basalt-derived Li. Indeed, we estimate that rainwater Li always represents less than 1% of the total Li. Few rainwater δ^7Li values have been published, but taking into account a δ^7Li value of 14.3‰ as reported in Pistiner and Henderson (2003) for a filtered Hawaiian rain, or a δ^7Li value of 31‰ in case of a seawater-like signature (Millot et al., 2007), such a flux would induce a shift of only 0.3‰. Even using the reported maximum δ^7Li value of 95.6‰ reported for polluted rainwater (Millot et al., 2010) would cause a small shift (0.9‰) of the soil δ^7Li value. In the same way, assuming that all the dust at the oldest site has remained in the profile without being weathered, with a δ^7Li value of 1.7‰ (UCC; Teng et al., 2009), this would represent a maximum increase of 0.6‰ of the soil δ^7Li value.

The small isotope shift induced by atmospheric additions is nowhere near as significant for Li as it is for some other ions such as Sr, and this is best explained by the strong preservation of basaltic Li through its incorporation into secondary clay minerals. This mechanism allows us to use this chronosequence to study the fate of Li along the time history of weathering, through the synthesis of metastable SRO minerals, and their transformation into relatively inert secondary minerals.

5.4. Controls of Li isotope fractionation during basalt alteration

As shown in Fig. 5, the negative δ^7Li values at the 20 and 150 ka sites are not explained by a simple source mixing. These values are therefore the consequence of significant Li isotope fractionation during weathering and associated secondary mineral formation processes. Although basalt dissolution is not expected to induce significant isotope fractionation (e.g., Pistiner and Henderson, 2003; Wimpenny et al., 2010a; Verney-Carron et al., 2011), formation of Fe oxides and clays at low temperature may result in large Li isotope fractionations, preferentially incorporating light Li (^{6}Li) into the solid phase (e.g., Williams and Hervig, 2005; Vigier et al., 2008; Wimpenny et al., 2010b). In more detail, depth-integrated δ^7Li, $\delta^7Li_{present}$, calculated using Eq. (2), highlights significant temporal variations (Fig. 6; Table 3). As shown in Fig. 6a, $Li_{present}$ also increases with age as the Li released from the parent basalt and added from atmospheric deposits also increases. The isotope composition of the Li released into waters by each regolith, δ^7Li_{loss} , can then be calculated as follows:

$$\delta^7Li_{loss} = \delta^7Li_{water} = \left(\frac{\delta^7Li_{total}\cdot Li_{total} - \delta^7Li_{present}\cdot Li_{present}}{Li_{loss}}\right), \quad (10)$$

δ^7Li_{water} is also quite variable as a function of time, ranging from 3.8‰ at the 4100 ka site to 11.3‰ at the 1400 ka site (Table 3).

Overall, the temporal evolution of Li and Li isotopes can be described in four main stages: (1) At the two youngest sites, $\delta^7Li_{present}$ is close to δ^7Li of the parent rock, despite ~30% Li loss by leaching, indicating that during the initial stage of basalt dissolution Li loss is not associated with significant Li isotope fractionation, in good agreement with experimental and other field studies (Pistiner and Henderson, 2003; Huh et al., 2004; Wimpenny et al., 2010a; Verney-Carron et al., 2011; Pogge von Strandmann et al., 2012; Liu et al., 2013). (2) The larger Li losses at the 20 ka and 150 ka sites ($\tau_{int} = -58\%$ and -49%, respectively; Fig. 3; Table 2) are associated with lower $\delta^7Li_{present}$ values. In Fig. 5, samples from the 20 and 150 ka sites define a single negative trend towards low δ^7Li values that can be interpreted as a preferential enrichment in ^{6}Li associated with Li incorporation into secondary phases. This process can also explain the smaller Li loss compared to other alkali elements at these sites (Fig. 3) because Li released by basalt dissolution is partially retained in secondary phases. From the mineralogical composition (Table S1; Ziegler et al., 2005), the 20 and 150 ka sites are distinct from the other sites because they both contain greater amounts of chemically active non-crystalline phases, such as allophane, imogolite and ferrihydrite. Our results therefore suggest that the formation of these phases plays a key role in the Li isotope compositions in these soils. (3) At 1400 ka, there is an increase of water δ^7Li (Fig. 6b), related to a significant increase of depth-integrated τ_{Li} (Fig. 3). This feature is consistent with a significant incorporation of Li into kaolinite, which is known to contain high Li levels (Tardy et al., 1972). As shown in Fig. 2a, kaolinite-rich horizons in this soil ($\geqslant$40 cm; Table S1) are also rich in Li (compared to two youngest soils), supporting this statement. These horizons display δ^7Li values that are slightly lower than the basalt value and the corresponding water δ^7Li value is estimated to be high (Fig. 6). This suggests a significant isotope fractionation during kaolinite formation, favoring the preferential incorporation of ^{6}Li into the solid. (4) Water δ^7Li then decreases between 1400 and 4100 ka and is associated with a significant loss of Li (Figs. 3 and 6). Kaolin-rich horizons at depth have clearly lost their Li since the abundance of kaolin minerals does not change from 1400 to 4100 ka (Table S1) but τ_{Li} significantly decreases (Fig. 2a). This significant loss of Li can also be seen from a bulk point of view in Fig. 3. It has almost no influence on the isotope signal at the depths where kaolin predominates (Fig. 2b), strongly suggesting no isotope fractionation during this Li release. This also explains well the decrease of water δ^7Li between the two oldest profiles exhibited in Fig. 6b.

It is interesting to note that the most elevated δ^7Li, measured in the upper layers (<30 cm) of the two oldest sites, are associated with high Nb/Li ratios (Fig. 5), and cannot be explained by atmospheric deposition, as described in the previous section. Furthermore, it cannot be simply related to secondary phase formation that would rather retain Li in the regolith. Such elevated δ^7Li values (>10‰) are particularly unusual in silicate soils. Huh et al. (2004) have also measured high δ^7Li in some samples of the Hawaiian climosequence, but they were clearly controlled by marine aerosols. The upper horizons of the 1400 and 4100 ka sites are enriched in organic matter (Table S1), but as a first approximation, we can rule out a key role of vegetation because of low Li levels in plants and the lack of associated isotope fractionation (Lemarchand et al., 2010). Since the surface soil horizons have lost some Li compared to younger soils (Fig. 2a), these heavy signatures have to be in the most resistant phases. As a first approximation, it seems possible that there has been Li isotope exchange with rainwater or with percolating soil solutions because that would explain inheritance of the heavy isotope signature without having to add significant amounts of Li to the soil budget. However, the remaining minerals at the surface of these old soils are particularly inert (Chorover et al., 2004) and therefore it would be surprising if rainwater exchange could strongly affect the Li isotope composition of these horizons. Another possibility would be a preferential release of ^{6}Li, either by isotope fractionation during clay alteration or by the preferential dissolution of low δ^7Li phases, leaving behind some secondary products, which did not fractionate Li isotopes when they formed. More detailed and experimental investigations are required to better understand these particularly heavy signatures in the surface horizons on the two oldest soils.

Although we show that non-linear evolution of the soil δ^7Li with age can be related to the mineralogical evolution of these soils, it is also interesting to note that the regolith δ^7Li value co-varies with a global climate proxy (δ^{18}O of benthic forams; Lisiecki and Raymo, 2005). Indeed, current

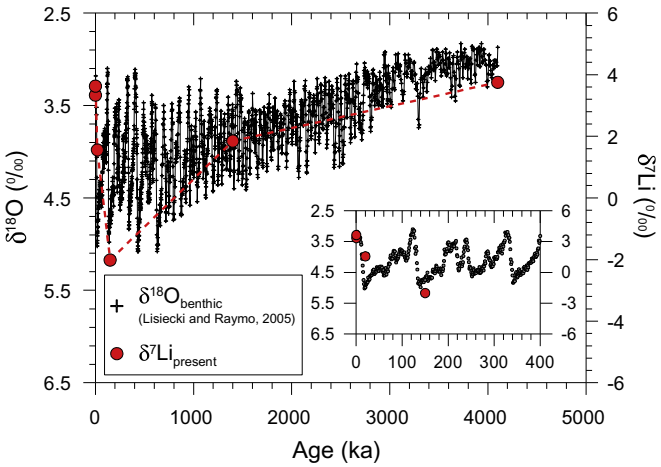

Fig. 7. δ^7Li of the present Li (on right axis) and δ^{18}O of benthic forams (on left axis) versus age. Benthic δ^{18}O values (on left axis) are from Lisiecki and Raymo (2005).

conditions on these sites are reasonably comparable, with $MAP = 2500$ mm and $T = 16$ °C on average, but if young sites have passed their entire life under interglacial conditions, the older sites have spent time in significantly different climate conditions (Hotchkiss et al., 2000). The 20, 150, and 1400 ka sites spent at most 40% of their histories under conditions similar to the modern interglacial, whereas the oldest 4100 ka site experienced the full range of Quaternary climate variation, plus warmer and wetter conditions in the Pliocene. Although this would need to be investigated with more data, the co-variation between δ^7Li and δ^{18}O indicates a possible control of climatic conditions on the soil δ^7Li, and therefore on the water δ^7Li values (Fig. 7). The soil δ^7Li is close to the value of the parent basalt at periods of time characterized by low δ^{18}O value, i.e., when global temperature was higher. This is consistent with more congruent release of Li isotopes during periods of more intensive weathering of the basaltic rocks, due to temperature increase. In contrast with continental record, the marine δ^7Li record (e.g., Hall et al., 2005; Hathorne and James, 2006; Misra and Froelich, 2012) cannot be used to reconstruct rapid weathering changes because of the long residence time of lithium in the ocean (>1 Ma). As a consequence, any short-term change of δ^7Li in the foraminifera can only be attributed to change of isotope fractionation during foraminifera growth and not due to change of sources or sinks.

6. CONCLUSIONS

The Hawaiian Islands LSAG chronosequence allows us to examine the processes responsible for changes in the Li isotope composition during progressive weathering and basaltic soil formation. We determine a small contribution from atmospheric deposits to the Li soil budget for all the sites, which frees us to explore the details of silicate mineral alteration processes on soil Li isotope signatures. The youngest soils (0.3 ka) at the Thurston (Th) and Ola'a (Ol) sites have the similar δ^7Li value as fresh basalt, indicating that basalt dissolution does not result in significant Li isotope fractionation during a period of 300 years. Older soils ($\geqslant$20 ka) display more variable δ^7Li values compatible with the known mineralogical and crystallographical evolution of these profiles. In particular, the Li uptake by non-crystalline phases, such as allophane, imogolite and ferrihydrite, and then by kaolinite play a key role. Finally, we suggest that the non-linear evolution of the bulk soil δ^7Li value as a function of time is consistent with a more congruent release of Li isotopes during warmer periods.

ACKNOWLEDGMENTS

The authors thank B.Y. Song and H.S. Shin for the analytical assistance. This work was supported by the KBSI Grants (F34610 and C34701) to J.-S.R. and by NSF-DEB-1020791 to O.A.C. Thoughtful comments from Paul Tomascak, X.-M. Liu, and Josh Wimpenny greatly improved the manuscript. We thank the Associate Editor Mark Rehkämper for handling the manuscript.

APPENDIX A. SUPPLEMENTARY DATA

Supplementary data associated with this article can be found, in the online version, at http://dx.doi.org/10.1016/j.gca.2014.08.030.

REFERENCES

Bern C. R., Brzezinski M. A., Beucher C., Ziegler K. and Chadwick O. A. (2010) Weathering, dust, and biocycling effects on soil silicon isotope ratios. *Geochim. Cosmochim. Acta* **74**, 876–889.

Berner R. A. (2004) *The Phanerozoic Carbon Cycle: CO_2 and O_2*. Oxford University Press.

Brady P. V. and Gíslason S. R. (1997) Seafloor weathering controls on atmospheric CO_2 and global climate. *Geochim. Cosmochim. Acta* **61**, 965–973.

Brimhall G. H. and Dietrich W. E. (1987) Constitutive mass balance relations between chemical composition, volume, density, porosity, and strain in metasomatic hydrochemical

systems: results on weathering and pedogenesis. *Geochim. Cosmochim. Acta* **51**, 567–587.
Chadwick O. A., Brimhall G. H. and Hendricks D. M. (1990) From a black to a gray box – a mass balance interpretation of pedogenesis. *Geomorphology* **3**, 369–390.
Chadwick O. A., Gavenda R. T., Kelly E. F., Ziegler K., Olson C. G., Elliott W. C. and Hendricks D. M. (2003) The impact of climate on the biogeochemical functioning of volcanic soils. *Chem. Geol.* **202**, 195–223.
Chadwick O. A., Derry L. A. and Vitousek P. M. (2009) Changing sources of strontium to soils and ecosystems across the Hawaiian Islands. *Chem. Geol.* **267**, 64–75.
Chan L. H. and Frey F. A. (2003) Lithium isotope geochemistry of the Hawaiian plume: results from the Hawaii Scientific Drilling Project and Koolau volcano. *Geochem. Geophys. Geosyst.* **4**, 8707. http://dx.doi.org/10.1029/2002GC000365.
Choi M. S., Ryu J. S., Park H. Y., Lee K. S., Kil Y. and Shin H. S. (2013) Precise determination of the lithium isotope ratio in geological samples using MC-ICP-MS with cool plasma. *J. Anal. At. Spectrom.* **28**, 505–509.
Chorover J., DeChiaro M. J. and Chadwick O. A. (1999) Structural charge and cesium retention in a chronosequence of tephritic soils. *Soil Sci. Soc. Am. J.* **63**, 169–177.
Chorover J., Amistandi M. K. and Chadwick O. A. (2004) Surface charge evolution of mineral–organic complexes during pedogenesis in Hawaiian basalt. *Geochim. Cosmochim. Acta* **68**, 4859–4876.
Crews T. E., Kitayama K., Fownes J. H., Riley R. H., Herbert D. A., Mueller-Dombois D. and Vrrousek P. M. (1995) Changes in soil phosphorus fractions and ecosystem dynamics across a long chronosequence in Hawaii. *Ecology* **76**, 1407–1424.
Dessert C., Dupré B., François L. M., Schott J., Gaillardet J., Chakrapani G. and Bajpai S. (2001) Erosion of Deccan Traps determined by river geochemistry: impact on the global climate and the $^{87}Sr/^{86}Sr$ ratio of seawater. *Earth Planet. Sci. Lett.* **188**, 459–474.
Dessert C., Dupré B., Gaillardet J., François L. M. and Allègre C. J. (2003) Basalt weathering laws and the impact of basalt weathering on the global carbon cycle. *Chem. Geol.* **202**, 257–273.
Fiske R. S., Rose T. R., Swanson D. A., Champion D. E. and McGeehin J. P. (2009) Kulanaokuaiki Tephra (ca. A.D. 400–1000): newly recognized evidence for highly explosive eruptions at Kilauea volcano, Hawaii. *Geol. Soc. Am. Bull.* **121**, 712–728.
Gislason S. R. and Eugster H. P. (1987) Meteoric water–basalt interactions. II: a field study in N.E. Iceland. *Geochim. Cosmochim. Acta* **51**, 2841–2855.
Gislason S. R. and Hans P. E. (1987) Meteoric water–basalt interactions. I: a laboratory study. *Geochim. Cosmochim. Acta* **51**, 2827–2840.
Goodfellow B. W., Hilley G. E. and Chadwick O. A. (2013) Depth and character of rock weathering across basalt-hosted climosequences on Hawaii and Kauai. *Earth Surf. Processes Landforms*. http://dx.doi.org/10.1002/esp.3505.
Hall J. M., Chan L.-H., McDonough W. F. and Turekian K. K. (2005) Determination of the lithium isotopic composition of planktic foraminifera and its application as a paleo-seawater proxy. *Mar. Geol.* **217**, 255–265.
Hathorne E. C. and James R. H. (2006) Temporal record of lithium in seawater: a tracer for silicate weathering? *Earth Planet. Sci. Lett.* **246**, 393–406.
Huang K. E., You C. F., Liu Y. H., Wang R. M., Lin P. Y. and Chung C. H. (2010) Low-memory, small sample size, accurate and high-precision determinations of lithium isotopic ratios in natural materials by MC-ICP-MS. *J. Anal. At. Spectrom.* **25**, 1019–1024.
Hotchkiss S., Vitousek P. M., Chadwick O. A. and Price J. (2000) Climate cycles, geomorphological change, and the interpretation of soil and ecosystem development. *Ecosystems* **3**, 522–533.
Huh Y., Chan L. H., Zhang L. and Edmond J. M. (1998) Lithium and its isotopes in major world rivers: implications for weathering and the oceanic budget. *Geochim. Cosmochim. Acta* **62**, 2039–2051.
Huh Y., Chan L. C. and Edmond J. M. (2001) Lithium isotopes as a probe of weathering processes: Orinoco river. *Earth Planet. Sci. Lett.* **194**, 189–199.
Huh Y., Chan L. H. and Chadwick O. A. (2004) Behavior of lithium and its isotopes during weathering of Hawaiian basalt. *Geochem. Geophys. Geosyst.* **5**, Q09002. http://dx.doi.org/10.1029/2004GC000729.
Jackson M. L., Levelt T. W. M., Syers J. K., Rex R. W., Clayton R. N., Sherman G. D. and Uehara G. (1971) Geomorphical relationships of tropospherically derived quartz in the soils of the Hawaiian Islands. *Soil Sci. Soc. Am. Proc.* **35**, 515–525.
Kennedy M. J., Chadwick O. A., Vitousek P. M., Derry L. A. and Hendricks D. M. (1998) Changing sources of base cations during ecosystem development, Hawaiian Islands. *Geology* **26**, 1015–1018.
Kisakürek B., Widdowson M. and James R. H. (2004) Behaviour of Li isotopes during continental weathering: the Bidar laterite profile, India. *Chem. Geol.* **212**, 27–44.
Krienitz M. S., Garbe-Schonberg C. D., Romer R. L., Meixner A., Haase K. M. and Stroncik N. A. (2012) Lithium isotope variations in ocean island basalts – implications for the development of mantle heterogeneity. *J. Petrol.* **53**, 2333–2347.
Kurtz A. C., Derry L. A., Chadwick O. A. and Alfano M. J. (2000) Refractory element mobility in volcanic soils. *Geology* **28**, 683–686.
Kurtz A. C., Derry L. A. and Chadwick O. A. (2001) Accretion of Asian dust to Hawaiian soils: isotopic, elemental, and mineral mass balances. *Geochim. Cosmochim. Acta* **65**, 1971–1983.
Kyte F. T., Leinen M., Ross Heath G. and Zhou L. (1993) Cenozoic sedimentation history of the central North Pacific: inferences from the elemental geochemistry of core LL44-GPC3. *Geochim. Cosmochim. Acta* **57**, 1719–1740.
Lemarchand E., Chabaux F., Vigier N., Millot R. and Pierret M.-C. (2010) Lithium isotope systematics in a forested granitic catchment (Strengbach, Vosges Mountains, France). *Geochim. Cosmochim. Acta* **74**, 4612–4628.
Lisiecki L. E. and Raymo M. E. (2005) A Pliocene–Pleistocene stack of 57 globally distributed benthic $\delta^{18}O$ records. *Paleoceanography* **20**, PA1003.
Liu X. L., Rudnick R. L., McDonough W. F. and Cummings M. L. (2013) Influence of chemical weathering on the composition of the continental crust: insights from Li and Nd isotopes in bauxite profiles developed on Columbia River Basalts. *Geochim. Cosmochim. Acta* **115**, 73–91.
Lohse K. A. and Dietrich W. E. (2005) Contrasting effects of soil development on hydrological properties and flow paths. *Water Resour. Res.* **41**, W12419.
Ludwing T., Marschall H. R., Pogge von Strandmann P. A. E., Shabaga B. M., Fayek M. and Hawthorne F. C. (2011) A secondary ion mass spectrometry (SIMS) re-evaluation of B and Li isotopic compositions of Cu-bearing elbaite from three global localities. *Mineral. Mag.* **75**, 2485–2494.
MacDonald G., Abbott A. T. and Peterson F. L. (1983) *Volcanoes in the Sea: The Geology of Hawaii*. University of Hawaii Press.
Magna T., Wiechert U. H. and Halliday A. N. (2004) Low-blank isotope ratio measurement of small samples of lithium using multiple-collector ICPMS. *Int. J. Mass Spectrom.* **239**, 67–76.
McPhie J., Walker G. P. L. and Christiansen R. L. (1990) Phreatomagmatic and phreatic fall and surge deposits from

explosions at Kilauea volcano, Hawaii, 1790 A.D.: Keanakakoi Ash Member. *Bull. Volcanol.* **52**, 334–354.

Millot R., Guerrot C. and Vigier N. (2007) Accurate and high-precision measurement of lithium isotopes in two reference materials by MC-ICP-MS. *Geostand. Geoanal. Res.* **28**, 153–159.

Millot R., Petelet-Giraud E., Guerrot C. and Négrel P. (2010) Multi-isotopic composition (δ^{seven}Li–δ^{11}B–δD–δ^{18}O) of rainwaters in France: origin and spatio-temporal characterization. *Appl. Geochem.* **25**, 1510–1524.

Misra S. and Froelich P. N. (2012) Lithium isotope history of cenozoic seawater: changes in silicate weathering and reverse weathering. *Science* **335**, 818–823.

Moriguti T. and Nakamura E. (1998) Across-arc variation of Li isotopes in lavas and implications for crust/mantle recycling at subduction zones. *Earth Planet. Sci. Lett.* **163**, 167–174.

Nishio Y. and Nakai S. I. (2002) Accurate and precise lithium isotopic determinations of igneous rock samples using multi-collector inductively coupled plasma mass spectrometry. *Anal. Chim. Acta* **456**, 271–281.

Pett-Ridge J. C., Monastra V., Derry L. A. and Chadwick O. A. (2007) Importance of atmospheric inputs and Fe-oxides in controlling soil uranium budgets and behavior along a Hawaiian chronosequence. *Chem. Geol.* **244**, 691–707.

Pistiner J. S. and Henderson G. M. (2003) Lithium-isotope fractionation during continental weathering processes. *Earth Planet. Sci. Lett.* **214**, 327–339.

Pogge von Strandmann P. A. E., Burton K. W., James R. H., van Calsteren P. and Gislason S. R. (2010) Assessing the role of climate on uranium and lithium isotope behaviour in rivers draining a basaltic terrain. *Chem. Geol.* **270**, 227–239.

Pogge von Strandmann P. A. E., Opfergelt S., Lai Y.-J., Sigfússon B., Gislason S. R. and Burton K. W. (2012) Lithium, magnesium and silicon isotope behaviour accompanying weathering in a basaltic soil and pore water profile in Iceland. *Earth Planet. Sci. Lett.* **339–340**, 11–23.

Porder S. and Chadwick O. A. (2009) Climate and soil-age constraints on nutrient uplift and retention by plants. *Ecology* **90**, 623–636.

Porder S., Hilley G. E. and Chadwick O. A. (2007) Chemical weathering, mass loss, and dust inputs across a climate by time matrix in the Hawaiian Islands. *Earth Planet. Sci. Lett.* **258**, 414–427.

Rex R. W., Sayers J. K., Jackson M. L. and Clayton R. L. (1969) Eolian origin of quartz in soils of Hawaiian Islands and in Pacific pelagic sediments. *Science* **163**, 277–334.

Rudnick R. L. and Gao S. (2003) Composition of the continental crust. In *Treatise on Geochemistry* (eds. D. H. Heinrich and K. T. Karl). Pergamon, Oxford, pp. 1–64.

Stewart B. W., Capo R. C. and Chadwick O. A. (2001) Effects of rainfall on weathering rate, base cation provenance, and Sr isotope composition of Hawaiian soils. *Geochim. Cosmochim. Acta* **65**, 1087–1099.

Swoboda S., Brunner M., Boulyga S. F., Galler P., Horacek M. and Prohaska T. (2008) Identification of Marchfeld asparagus using Sr isotope ratio measurements by MC-ICP-MS. *Anal. Bioanal. Chem.* **390**, 487–494.

Tardy Y., Kremp G. and Trauth N. (1972) Le lithium dans les mineraux argileux des sediments et des sols. *Geochim. Cosmochim. Acta* **36**, 397–412.

Teng F. Z., McDonough W. F., Rudnick R. L., Dalpe C., Tomascak P. B., Chappell B. W. and Gao S. (2004) Lithium isotopic composition and concentration of the upper continental crust. *Geochim. Cosmochim. Acta* **68**, 4167–4178.

Teng F. Z., Rudge J. F., McDonough W. F. and Wu F. Y. (2009) Lithium isotopic systematics of A-type granites and their mafic enclaves: further constraints on the Li isotopic composition of the continental crust. *Chem. Geol.* **262**, 370–379.

Tomascak P. B., Carlson R. W. and Shirey S. B. (1999) Accurate and precise determination of Li isotopic compositions by multi-collector sector ICP-MS. *Chem. Geol.* **158**, 145–154.

Tomascak P. B., Langmuir C. H., le Roux P. J. and Shirey S. B. (2008) Lithium isotopes in global mid-ocean ridge basalts. *Geochim. Cosmochim. Acta* **72**, 1626–1637.

Verney-Carron A., Vigier N. and Millot R. (2011) Experimental determination of the role of diffusion on Li isotope fractionation during basaltic glass weathering. *Geochim. Cosmochim. Acta* **75**, 3452–3468.

Vigier N., Decarreau A., Millot R., Carignan J., Petit S. and France-Lanord C. (2008) Quantifying Li isotope fractionation during smectite formation and implications for the Li cycle. *Geochim. Cosmochim. Acta* **72**, 780–792.

Vigier N., Gislason S. R., Burton K. W., Millot R. and Mokadem F. (2009) The relationship between riverine lithium isotope composition and silicate weathering rates in Iceland. *Earth Planet. Sci. Lett.* **287**, 434–441.

Vitousek P. M. (2004) *Nutrient cycling and limitation: Hawaii as a model system*. Princeton University Press, Princeton, New Jersey, USA.

Vitousek P. M. and Chadwick O. A. (2013) Pedogenic thresholds and soil process domains in basalt-derived soils. *Ecosystems* **16**, 1379–1395.

Vitousek P. M., Chadwick O. A., Crews T. E., Fownes J. H., Hendricks D. M. and Herbert D. (1997) Soil and ecosystem development across the Hawaiian Islands. *GSA Today* **7**, 1–9.

Walker J. C. G., Hays P. B. and Kasting J. F. (1981) A negative feedback mechanism for the long-term stabilization of Earth's surface temperature. *J. Geophys. Res.* **86**, 9776–9782.

Wiegand B. A., Chadwick O. A., Vitousek P. M. and Wooden J. L. (2005) Ca cycling and isotopic fluxes in forested ecosystems in Hawaii. *Geophys. Res. Lett.* **32**, 1–4.

Williams L. B. and Hervig R. L. (2005) Lithium and boron isotopes in illite–smectite: the importance of crystal size. *Geochim. Cosmochim. Acta* **69**, 5705–5716.

Wimpenny J., Gislason S. R., James R. H., Gannoun A., Pogge Von Strandmann P. A. E. and Burton K. W. (2010a) The behaviour of Li and Mg isotopes during primary phase dissolution and secondary mineral formation in basalt. *Geochim. Cosmochim. Acta* **74**, 5259–5279.

Wimpenny J., James R. H., Burton K. W., Gannoun A., Mokadem F. and Gislason S. R. (2010b) Glacial effects on weathering processes: new insights from the elemental and lithium isotopic composition of West Greenland rivers. *Earth Planet. Sci. Lett.* **290**, 427–437.

Wolfe E. W. and Morris J. (1996) *Geologic Map of the Island of Hawaii*. US Geological Survey Miscellaneous Investigations Map I-2524.

Wright T. L. and Heltz R. T. (1986) Differentiation and magma mixing on Kilauea's east rift zone: a further look at the eruptions of 1955 and 1960. Part II. The 1960 lavas. *Bull. Volcanol.* **57**, 602–630.

You C.-F. and Chan L. H. (1996) Precise determination of lithium isotopic composition in low concentration natural samples. *Geochim. Cosmochim. Acta* **60**, 909–915.

Ziegler K., Chadwick O. A., Brzezinski M. A. and Kelly E. F. (2005) Natural variations of δ^{30}Si ratios during progressive basalt weathering, Hawaiian Islands. *Geochim. Cosmochim. Acta* **69**, 4597–4610.

Associate editor: Marc Norman